An attempt to predict spray characteristics at early stage of the atomization process by using surface density and curvature distribution

L. Palanti, S. Puggelli, L. Langone, A. Andreini, J. Reveillon, Benjamin Duret, F.X. Demoulin

An attempt to predict spray characteristics at early stage of the atomization process by using surface density and curvature distribution

L. Palanti[a,*], S. Puggelli[a], L. Langone[a], A. Andreini[a], J. Reveillon[b], B. Duret[b], F.X. Demoulin[b]

[a] *Department of Industrial Engineering (DIEF), University of Florence, via S. Marta 3, Florence 50139, Italy*
[b] *CORIA-UMR 6614, Normandie University, CNRS-University and INSA of Rouen, Avenue de l'Université BP 12, Saint-Étienne-du-Rouvray 76800, France*

Abstract

Nowadays, numerical simulations of atomization has reached a mature state through interface capturing approaches. With these approaches, the liquid-gas flow with its complex interface morphology can be precisely described but at the price of high mesh resolution, that makes these simulations very intensive in terms of computational cost. Practically, for most of the injection system, it is not possible to achieve a simulation up to a point where the spray formation is completed. Thus, there are several attempts based on the transformation of liquid elements such as ligaments, liquid sheet or other non-spherical to equivalent droplets. Overall, these approaches assumed that before the complete finalization of the atomization process the spray under formation carries enough information to be representative of the final spray. In this work, we have pushed this idea a step further by using global variables such as the liquid volume fraction and the surface density available in ELSA models to ensure the transports and the conservation of the main features of the spray. Then, the surface curvature distribution is analyzed assuming that a part of the interface carries already

*Corresponding author
Email address: lorenzo.palanti@htc.unifi.it (L. Palanti)

curvatures that are relevant with respect to the final spray. A well-known academic test case representative of an aeronautical injection system and based on a planar prefilmer atomizer with a gas co-flow has been selected to evaluate our proposal. This configuration was studied both experimentally and numerically thanks to high-fidelity simulations. Our purpose has been to follow the already validated numerical approaches but with less computationally intensive simulations. Then, new analysis based on surface density and surface curvature distribution have been tested to recover spray characteristics and even the spray diameter distribution. It appears that these variables are meaningful even when there is no droplet yet formed, and thus they allow the description of the full atomization process from the early stage even on the liquid film. Finally, a procedure has been proposed where the spray is sufficiently atomized to reconstruct the diameter distribution from the curvature distribution. At our best knowledge, this last step is a first attempt on practical injection system. We have proposed a very simple method to detect which part of the interface carries the relevant curvature, thus obtaining a reconstructed diameter distribution that fit well with available experimental data. Although the proposed approach cannot be still considered universally applicable to any case, this preliminary assessment clearly shows its potential.

Key words: Primary Breakup, Density of Interface, Interface Curvature, Drop Size Distribution, VoF

---

1. Introduction

In the last decades, numerical simulations gained a primary role in the design and development of aircraft burners. At the present day, Large Eddy Simulations (LES) coupled with advanced turbulent combustion models represent the the state of the art among other simulation techniques [11, 19]. However, primary liquid atomization still represents a rather complex task to handle numerically and usually it is not directly included in such simulations [11]. In fact, during the simulation of real engines or laboratory test rigs, the initial

breakup is often neglected and spherical droplets are directly injected assuming a prescribed velocity and a certain size distribution [32].

In this framework, large research efforts have been dedicated to the development both of Eulerian-Lagrangian (E-L) and Eulerian-Eulerian (E-E) methods for the dispersed region of the spray [32]. Despite strong assumptions (e.g., the mutual effect of flame on primary breakup is overlooked, evaporation in the dense zone is not accounted for, etc.) such approach still represents the most efficient and practical way to set up a reactive simulation of a complete burner. The main drawback of this procedure is represented by the need for experimental data or the availability/accuracy of empirical correlations to set up the initial injection conditions. Approaches based on the coupled solution of early spray development and combustion process might be considered, but they are still too expensive for LES of realistic geometries.

A viable alternative is represented by the use of separate detailed simulations of the primary breakup to obtain the initial conditions for spray injection in reactive LES. In this way, a large increase in the overall computational resources must be expected as well as a higher accuracy and reliability of the obtained spray characteristics. In the scientific literature, there are already several works dealing with detailed simulations of the primary liquid atomization in the aero-engine context. Several configurations of interest have already been studied, like jets in cross-flow [20, 27], swirl atomizers [14, 35] and prefilming airblast atomizers [5, 33, 34, 38]. A complete review of primary breakup simulations is out of the scope of this work and the interested reader is addressed to a recent review by Shinjo [36].

In this work, the experimental test case investigated by Gepperth and coworkers [16–18] has been simulated. It consists of a planar prefilmer atomizer operated at ambient pressure where measurements of droplet size distribution are available, as well as data about ligament formation. Moreover, shadowgraphy has been used to highlight the main structures formed during the breakup events.

From a numerical perspective, such rig is the subject of the recent work by Braun et al. [5], where the Smoothed Particle Hydrodynamics (SPH) method

has been used to simulate in detail the liquid structures originated by the primary breakup. Thanks to a reported mean inter-particle distance of 5 μm, even very small liquid structures are captured and the primary atomization process is represented very accurately. The same test case has been investigated by Warncke et al. [38] using the native Volume of Fluid (VoF) approach of OpenFOAM ® (i.e., `interFoam`). Even in this case, thanks to a grid sizing below 10 μm, the breakup process is displayed with a very high definition.

Despite the promising results in terms of computational requirements shown in [5], in particular if compared against *traditional* finite volume methods, the overall amount of resources needed in [5, 38] is very large and probably beyond the reasonable limits of an engineering/industrial context.

Therefore, in this work a different strategy based on LES is used as an alternative, clearly with lower expectations in terms of accuracy, but more affordable at the present day.

A recent LES implementation of the Eulerian Lagrangian Spray Atomization model presented by Anez et al. [2] represents the starting point to simulate primary atomization. A complete review of the various developments and branches of the ELSA approach (often referred also as $\Sigma - Y$ or $\Omega - Y$) is beyond the scope of this work and the interested reader is addressed to [1, 24] and references therein. The main advantage of the coupled LES-ELSA formulation in dealing with this problem is the reduced computational effort ensured by the automated switch from Interface Capturing Method (ICM) to a diffused interface method based on ELSA. Despite the fact that here only the ICM part is of interest, such automated switch could be useful for future investigations under higher operating pressure (for instance [8]) where interface discretization could be computationally too expensive.

It is important to highlight that the ELSA approach has been extensively validated on liquid jets characterized by high Reynolds/Weber numbers such as *Diesel-like* injectors (for instance [1, 12, 40] on ECN spray A [15] or [29] on general diesel injectors) whereas a smaller effort has been devoted to other atomization devices. Few works have been addressed towards the simulation of

Jet In Cross-flow (JCF) atomization [23] and air-assisted atomization devices [3, 37]. At the best of the author knowledge, this is the first attempt to apply the ELSA model to the study of a prefilming airblast atomizer.

Regarding the postprocessing technique, in the work of Braun et Al. [5] the use of SPH allows a straightforward handling of phase interfaces.

To postprocess the simulation, gaseous particles are firstly removed to reduce the memory requirements and an enclosing surface mesh is extracted based on the remaining liquid particles. Then, tessellation is performed using the α-shape algorithm and the resulting triangulated surface is fed into a cluster detection algorithm based on the Connected Component Labeling (CCL) [31]. In this way, each cluster can be analysed individually: the clusters having an almost spherical shape are considered to compute spray statistics.

Similarly, in [38], to quantitatively postprocess the simulation, a sampling plane at the domain outlet is defined and a CCL algorithm is again used to detect connected liquid structures based on a certain minimum volume fraction in each cell. In this way, the number of formed droplets can be determined. Moreover, once a connected structure is detected, the surface area of each one is quantified by the sum of all cells containing liquid with the corresponding volume fraction and the grid size. Finally, the droplet diameter is derived by assuming a circular section. It is worth pointing out that, in this case, the final result is also influenced by the minimum liquid volume fraction value (or threshold) chosen to carry out the detection.

The common idea behind the reported examples is to carry out droplet identification by a clustering algorithm, which introduces the need to store a large amount of data [5] and to assume a certain threshold of liquid volume fraction [38].

In the present work, a novel attempt to characterize the spray formed by the atomization is presented. It is based on the analysis at runtime of global variables already available in ELSA approach, namely the liquid volume fraction (α_l from now on), the density of interface Σ and the interface curvature K. At first, the ratio between the transported α_l and Σ is used to estimate eventually

the Sauter Mean Diameter (SMD) over some sample planes in the attempt of monitoring the progress of the atomization process. Such step does not require the interface to be well captured and therefore it can be applied to ELSA simulations without strictly requiring ICM. Secondly, Σ and K are used to draw the interface distribution per classes of curvature. The study of this function will provide a complementary insight for the analysis of the breakup process. At this stage, ICM is required to evaluate K properly. Finally, this two sets of data are combined in a first attempt of extracting the Droplet Size Distribution (DSD) of the spray at the smallest distance from the injector to recover the main spray characteristics obtained experimentally. This approach is inspired of the work propose by Canu et al. [7]. Since this is the first attempt at our best knowledge to reconstruct the DSD from the interface distribution per classes of curvature, there is of course many shortcomings that are justified at this stage by our will to provide a method based on the tools presently available in the most of liquid-gas simulations used in this field of application. Meanwhile, further research development is ongoing on many points to better approximate the curvature distribution, that will provide additional improvements when available. As well, further test cases will be investigated aiming to understand if this novel approach can be generalized to different injection systems and operating conditions. However, at this point, the focus remains the evaluation of the information available at a certain stage of the atomization with a reduced numerical resolution and without the introduction of further quantities.

The paper is structured as follows: the numerical approach employed to carry out the simulation and the strategy adopted to post-process it are first introduced. Then, the investigated test case is presented, as well as the specific numerical setup to simulate it. A set of *raw* results are shown in the following chapter by using interface density to probe the Sauter mean diameter and to probe the curvature distribution. Finally, a new analysis is carried out to test the possibility to determine the spray DSD even at this early stage of the atomization process. At the very end, conclusions are made pointing out the potential development of this work and the following perspectives.

2. Numerical approach

2.1. Multiphase ELSA solver

The multiphase model presented by Anez et al. [1] has been employed with minor modifications. Therefore, in this paragraph only a brief description is provided and the reader interested in a deeper overview of the ELSA approach and in examining all the governing equations is addressed to the aforementioned reference [1].

The employed `icmElsaFoam` solver is a LES-based approach where the standard `interFoam` solver of OpenFOAM ® is coupled with the ELSA approach: in the first one, the interface between liquid and gas must be *captured* whereas, in ELSA, the interface position is *non-resolved* and must be represented at sub-grid level and *modelled*. To continuously switch from one approach to the other, within the same computational domain, two *Interface Resolved Quality* (IRQ) sensors have been introduced in [1].

Since, in this work, our effort is devoted to the *captured* part, IRQ sensors have been used only to assess if the employed grid size is sufficient to *resolve* most of the turbulent fluctuations taking place at the interface between liquid and gas: if not, local results have been discarded. This point will be clarified once the computational grid is introduced.

In [1] the overall density of interface Σ has been split into two components, namely $\Sigma = \Sigma_{min} + \Sigma^{'}$. In this expression Σ_{min} represents the density of the interface related to the presence of any fraction of liquid within the control volume (even under laminar conditions), while $\Sigma^{'}$ is the amount of additional interface produced by sub-grid fluctuations. A sketch of this idea is shown in Fig. 1. $\Sigma^{'}$ is transported across the computational domain using Eqn. 1:

$$\frac{\partial \Sigma'}{\partial t} + \nabla \cdot \left(\overline{\boldsymbol{U}} \Sigma'\right) = \nabla \cdot \left[\frac{\nu_t}{Sc_t} \nabla \Sigma'\right] + C_\Sigma \frac{\Sigma}{\tau_\Sigma} \left(1 - \frac{\Sigma}{\Sigma^*}\right), \tag{1}$$

where $\overline{\boldsymbol{U}}$ is the resolved velocity of the mixture, ν_t and Sc_t are the turbulent subgrid viscosity and the Schmidt number respectively. The source term on the RHS is designed so that the overall density of interface Σ tends to an equilibrium

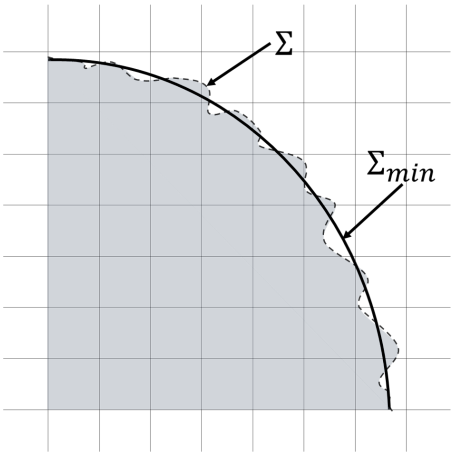

Figure 1: Sketch of the variables used for interface description: Σ is the overall density of the interface composed of Σ_{min} and $\Sigma^{'}$.

value Σ^* over a certain time scale τ_Σ. The unknown terms closure used by Anez et al. [1] is here retained. The reader interested in further details on this topic is addressed to the provided reference.

Compared to [1] only a different definition of Σ_{min} has been preferred here (Equation 2), as it is known to produce a better estimation of the density of the interface when the interface is *captured*:

$$\Sigma_{min} = |\nabla \overline{\alpha}_l|, \tag{2}$$

where $\overline{\alpha}_l$ stands for the LES-filtered liquid volume fraction, which is tracked within the computational domain using a dedicated equation (see [1] for reference).

As it will be clarified later, only the resolved (ICM) part is considered in this work. The reader might argue that there was no need to adopt the coupled solver `icmElsaFoam` rather than `interFoam`. The main advantage of using this framework lies in the availability of the already mentioned IRQ sensors, which allows to understand when the liquid phase is *sufficiently* well captured to trust the output of the ICM technique, or when a purely diffused interface approach must be considered without interface straightening method. Moreover, com-

pared to standard `interFoam` solver, `icmElsaFoam` only includes the solution of an additional equation, which does not dramatically increase the required computational effort. For the considered test case, as shown in [38], a finer mesh could be necessary to *well-capture* the interface compared to the one used here. This would be in contrast with the engineering purpose of the present work, which focuses on a cost-effective and affordable method to extract spray characteristic from CFD, rather than rely on experimental correlations or experiments. To this aim, a relatively coarse mesh is used in the the whole domain while a higher refinement is applied in the atomization region. Anyway, there is still no way to determine whether liquid structures are *well-captured* or not, also considering that mesh requirements may vary in time due to large velocity fluctuations. Moreover, as soon as the break up or coalescence occurs, the smallest length scale of the interface tends to zero. Thus, it is in principle impossible to reach a mesh resolution that cover all scale of the interface. Considering this, the objective is restricted to achieve a mesh resolution high enough to capture certain properties of the flow, hence computing SMD and surface curvature distribution[6] Here, `icmElsaFoam` provides the previously mentioned IRQs, that determine the reliability of the ICM method.

We have observed that IRQs are always met (i.e., the interface resolution is enough to apply the ICM) in the refined region, while they are not outside, and thus no data are collected over there.

2.2. SMD calculation

The novel post-processing technique is composed of two stages. First, the density of interface Σ is used together with the liquid volume fraction α_l to compute the SMD then, the mean curvature K distribution is employed to obtain the DSD.

It is worth pointing out again that, to apply the proposed procedure, it is not necessary to store several instantaneous snapshots of liquid distributions. Moreover, compared to other approaches based on a VoF method, the technique is not dependent on the assumed threshold of liquid volume fraction used to

carry out the identification of the droplets.

The SMD (D_{32} in equations) of a spray is defined as the ratio between the amount of liquid volume and its surface [22]. Based on that, two definitions can be introduced depending on the strategy used to track the liquid phase. If information about single droplets is available, it is convenient to calculate the SMD as (Equation 3):

$$D_{32}^{L} = \frac{\sum_i D_{p,i}^3}{\sum_i D_{p,i}^2} = 6\frac{V_l}{A_l} \tag{3}$$

where $D_{p,i}$ is the diameter of the i-th droplet, whereas V_l and A_l are respectively the volume and the area of the considered portion of spray.

On the other hand, using the variables introduced so far by the ELSA approach, if a control volume V is considered, then the D_{32} can be computed integrating (Equation 4):

$$D_{32}^{E}(V) = 6\frac{V_l}{A_l} = 6\frac{\iiint_V \overline{\alpha}_l dv}{\iiint_V \Sigma dv} \tag{4}$$

where dv stands for the volume element of the integration. In Figure 2 the difference between D_{32}^{L} and D_{32}^{E} is graphically explained. D_{32}^{L} can be used

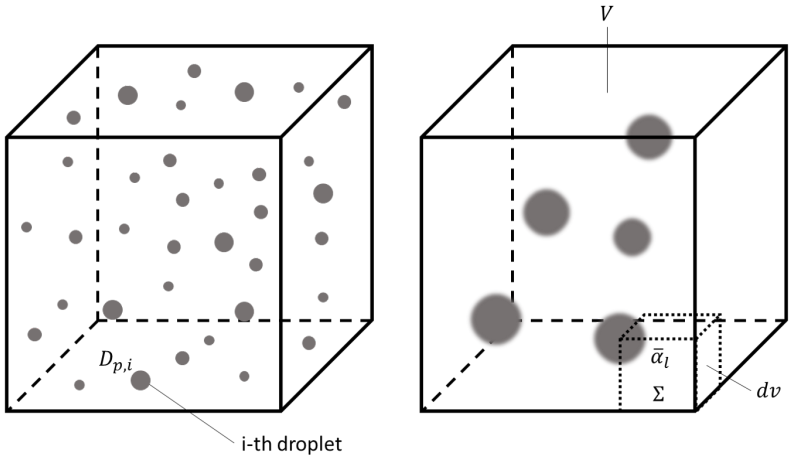

Figure 2: Conceptual difference between Sauter diameter definitions. Left: based on discrete droplet diameters (D_{32}^{L} - Equation 3), right: based on phase indicator α_l and interface density (D_{32}^{E} - Equation 4).

in experimental measurements, E-L simulations or ICM computations through

interface recognition, but it cannot be directly adopted in simulations where either there is an uncertainty on the interface position, or the spray is composed by a set of liquid parcel not fully spherical and well identified. On the other hand, D_{32}^E can be directly adopted in the considered framework, without requiring additional considerations on droplet identification. From a theoretical point of view, if $\overline{\alpha}_l$ and Σ are well determined and if the spray is composed of spherical droplet, the two definitions should lead to the same result, i.e. $D_{32}^L = D_{32}^E$.
From a simulation point of view, it is usually more convenient to compute the SMD of the droplets flowing trough a given plane S. Therefore, starting from Equation 4, Equation 5 can be written:

$$D_{32}^E(S) = 6\frac{\int_T \iint_S (\overline{\alpha}_l \boldsymbol{U} \cdot \vec{n} ds) dt}{\int_T \iint_S (\Sigma \boldsymbol{U} \cdot \vec{n} ds) dt} \tag{5}$$

where S stands for the surface over which a time average SMD is computed within the timeframe T. $\vec{n}$ is the normal to the surface S and therefore $\boldsymbol{U} \cdot \vec{n}$ is the component of the mixture velocity normal to S. This also corresponds to the output that is usually available from experiments, where only particles crossing a certain plane are considered. A sketch of this concept is provided in Figure 3 (left).

While this already represents an interesting way to compute the SMD for a given plane, SMD distributions in space could be of use rather than a uniform value (e.g. for non-uniform injection of Lagrangian droplets in space or just to compare against experiments).
In this work, the SMD distribution has been computed also over discrete lines. Given a certain reference frame (x, y, z), the SMD variation along y can be computed for a constant value of x_0 by integrating over z as follows:

$$D_{32}^E(x_0, y) = 6\frac{\int_T \int_{z_1}^{z_2} (\overline{\alpha}_l(x_0, y, z) \boldsymbol{U}(x_0, y, z) \cdot \vec{x} dz) dt}{\int_T \int_{z_1}^{z_2} (\Sigma(x_0, y, z) \boldsymbol{U}(x_0, y, z) \cdot \vec{x} dz) dt} \tag{6}$$

Equation 6 is illustrated in Figure 3 (right).

The output of the presented equation will be clarified in the next sections, but it is now worth mentioning its potential. For instance, if a simplex atomizer is considered, with an axisymmetric design, the radial SMD variation could be

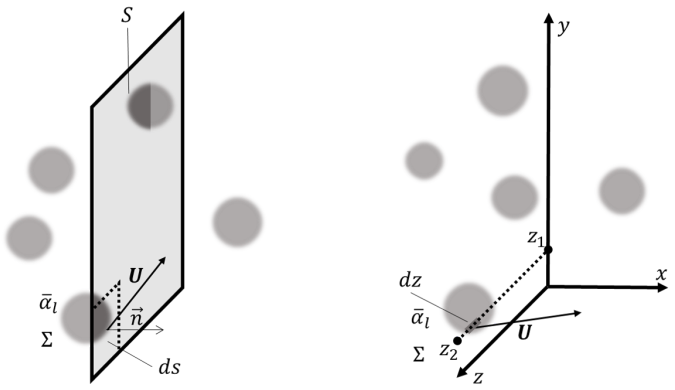

Figure 3: Graphical representation of the post-processing technique applied to compute the SMD: left, over discrete planes (Equation 5) and right, over discrete lines (Equation 6).

computed at a certain axial distance from the injector, providing also an idea of the angular dispersion of the spray.

The presented approach is quite general although it requires the native variables of the `icmElsaFoam` model. Its application to a planar prefilmer experimental test case is shown in the next sections.

2.3. Estimation of the curvature

While in the previous section we proposed a way to estimate the SMD, no information is yet available on the size distribution of the generated spray. Nevertheless, very different distributions can still provide the same SMD but largely affect the final flame shape due to the different evaporation and combustion time-scales associated to each class of diameter. In this work, we also propose an approach to extract spray distribution by analyzing the liquid/gas interface mean curvature K.

The reader interested to an exhaustive discussion about curvature in sprays is addressed to specific literature (see [7] and references therein). Hereby, the idea introduced in [7] on a Homogeneous Isotropic Turbulence (HIT) box to extract the DSD is exploited on a more complex test case. In [7] the Gauss $G = k_1 * k_2$

and the mean $H = \frac{k_1+k_2}{2}$ curvatures have been computed from the two principal curvatures of the surface k_1 and k_2, following the method presented in [21].

To this aim, the two principal curvatures have been computed with two different post-processing techniques: the first one is based on the level-set function available in the employed solver ARCHER [25], while the second one is presented in [26] and based on gas-liquid interface discretization with a 2D triangulated mesh.

While in [7], several detailed analysis on liquid curvature evolution have been carried out, here we focus our analysis of curvature to characterize the primary-breakup process on a configuration of technical interest for applications. At our best knowledge to use curvature distribution to predict spray characteristics has never been published before.Here, our aim is to study what is the benefit of curvature distribution analysis first with standard output of any CFD codes devoted to liquid-gas flow. They necessarily have internal determination of curvature to evaluate surface tension force. As previously discussed there is room for improvement by using more detailed strategies for estimating the curvature. Though, it would go beyond the scope in this work where we will see which information can be extracted of standard approaches. Our purpose, instead, is to study if it is possible to benefit of curvature analysis and surface density measurement to approximate the SMD and the DSD with a simulation that is less demanding than the reference high fidelity simulations carried out by other research groups [5] [38] .

Accordingly, the analysis is restricted to the total curvature already implemented in any ICM approach to compute surface tension force:

$$K = -\nabla \cdot \left(\frac{\nabla \overline{\alpha}_l}{|\nabla \overline{\alpha}_l|} \right) \tag{7}$$

The reader interested in a detailed review of curvature computation in OpenFOAM is addressed to specific literature [4, 13].

Similarly to [7], the total curvature K space is split in several classes corresponding to the different intervals of possible K. On each of them the amount

of surface area carrying the curvature K is accumulated and stored. From now on, this distribution will be referred as Surface Curvature Distribution (SCD). Therefore, despite K being defined everywhere, the PDF is actually populated only when the amount of surface $A_K = \Sigma\, dv \neq 0.0$ and therefore interface can be found. Such procedure has been coded in OpenFOAM by directly storing at runtime the A_K associated to predefined classes of curvature K in a predefined probe volume. The choice of such probe volume will be discussed in the next session, once the investigated test case has been presented. Finally, to ensure an accurate estimation of the liquid-gas surface normal and its divergence a smooth function describing the phase transition is expected. Accurate result have been obtained in [7] by using the distance function in `icmElsaFoam`. Such function is not available in all codes and in particular within `interFoam`, but we have been able to recover the curvature even when liquid interface is not perfectly localized, but smeared over a few cells following the work of [13]. The next section presents the test case of interest and the liquid-gas simulation set up by following previous published approaches, but with less demanding mesh resolution. Then, the first analysis of the break-up based on the estimated Sauter mean diameter is conducted before to address the possibility to estimate the DSD base on the curvature distribution.

3. Investigated test case

3.1. Experimental setup

The numerical methods presented in Section 2 have been applied to investigate the planar prefilming airblast atomizer experimentally studied at the Institut für Thermische Strömungsmaschines (ITS) of the Karlsruhe Institute of Technology (KIT) [8, 16–18, 38]. A sketch of the test section is reported in Figure 4. The geometry consists in a planar wing-shaped prefilmer where the liquid is supplied through a cavity on one side of the prefilmer body. The injection is performed using 50 equidistant distributed holes, forming a thin film of liquid that homogeneously wets the surface up to the atomizing edge. Here,

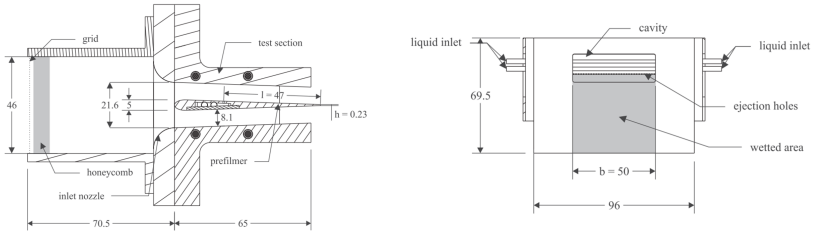

Figure 4: Experimental setup of the prefilmer for the KIT atomizer: side view (left) and top view (right). Adapted from [38].

the liquid accumulates and creates a liquid reservoir that feeds the atomization process whereas the air flows around the wing-shaped geometry on both sides. Available measurements include particle and ligament tracking as well as Laser Doppler Anemometry. But, above all, the shadowgraphy technique has been used to acquire information about the amount of liquid accumulation at the prefilming edge and collect statistics about the generated droplets and ligaments. A Depth of Field (DoF) correction has been employed to properly estimate the object sizes.

In this work, ambient pressure has been considered, with a nominal gas phase velocity of 40.0 m/s. Several liquids have been investigated experimentally, but in this case *Shellsol D70* has been selected for the simulation. The reported thickness of the prefilmer trailing edge is 230.0 μm. A summary of the operating conditions is reported in Table 1.

3.2. Preliminary single phase simulations

The great influence of the gaseous flow field on the atomization process leads to the requirement of accurate, time-dependent boundary conditions. In [38, 39], the concept of embedded DNS [33, 34] is exploited to obtain high-fidelity time-dependent BCs for the gaseous phase, in order to take into account the turbulent fluctuations generated inside the prefilmer channel. A similar strategy has been adopted here: at first, a single-phase LES of the whole prefilmer apparatus has been performed. Simulation velocity profiles at 0.3 mm downstream the

Table 1: Operating conditions and liquid fuel properties considered in the numerical simulation.

Gas phase velocity	40 m/s
Gas phase density	1.225 kg/m^3
Gas phase kinematic viscosity	1.48 e^{-05} m^2/s
Liquid phase velocity	0.5 m/s
Liquid phase density	770 kg/m^3
Liquid phase kinematic viscosity	2.026 e^{-06} m^2/s
Liquid phase surface tension	0.0275 kg/s^2
Prefilmer edge thickness	230 μm

atomizing edge are compared to the experiments in Figure 5. A good agreement is achieved both in terms of mean velocity and RMS. Then, the instantaneous

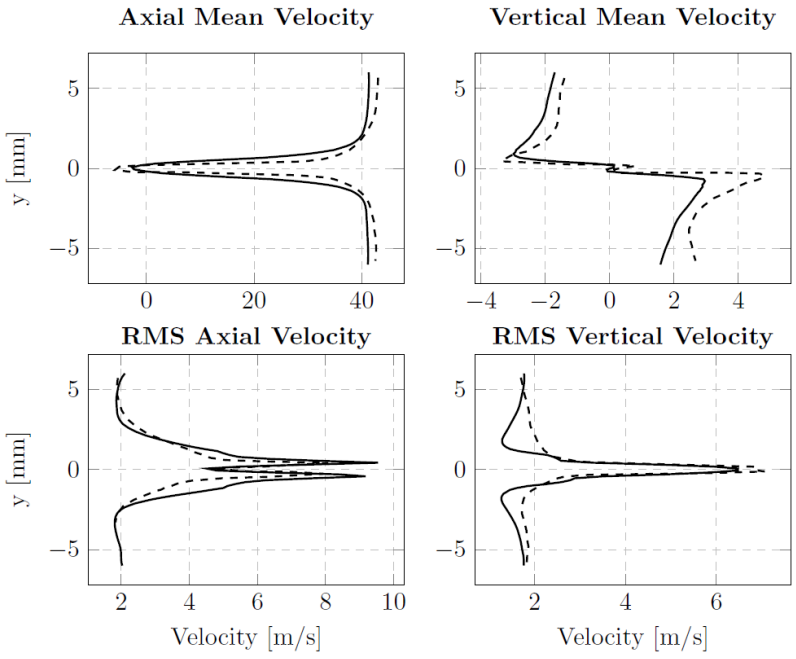

Figure 5: Comparison between the single-phase numerical simulation (plain line) and the experimental data (dotted line) 0.3 mm downstream the atomizing edge.

velocity vectors have been recorded on a plane and used as BCs for a second single phase simulation, similar to the *turbulent channel* used in [38]. This intermediate step is necessary to increase the definition of turbulent eddies close to the wall and the boundary layer. Again, a LES has been performed and velocity vectors have been stored to be used in the final ICM-ELSA simulation (see Section 3.3). A sketch of the strategy is reported in Figure 6. More details

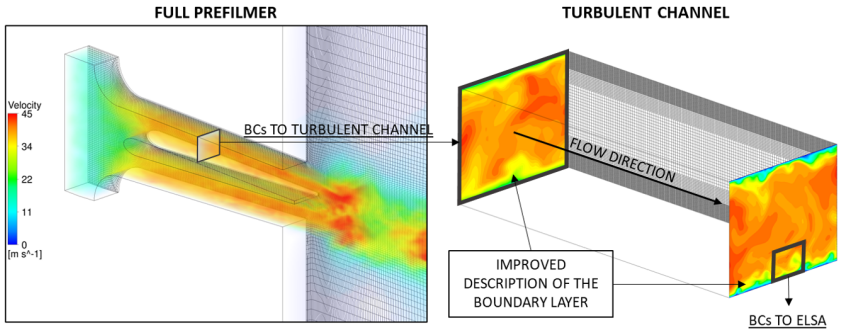

Figure 6: Schematic representation of the two mapping procedures carried out to obtain time varying velocity BCs for the ELSA simulation.

about the setup of single phase simulations can be found in Appendix 1.

3.3. Numerical setup of the ELSA computation

Following the work of Warncke et Al. [38], the multiphase simulation has been performed on a reduced domain representative of the last section of the prefilming edge (Figure 7). Two inlets are present for the gas phase, where the air velocity has been prescribed following time-varying profiles mapped within Section 3.2. Liquid is injected through a dedicated inlet (0.10 mm thick) with imposed mass flow rate and a uniform velocity profile. Therefore, the liquid flows over the prefilmer which is treated as a no-slip wall. The discretized section of the prefilmer is 1.00 mm long and 0.230 mm thick. The chosen length, allows to consider the formation of small waves (observed also in [38]) which may influence the atomization process whereas the thickness has been

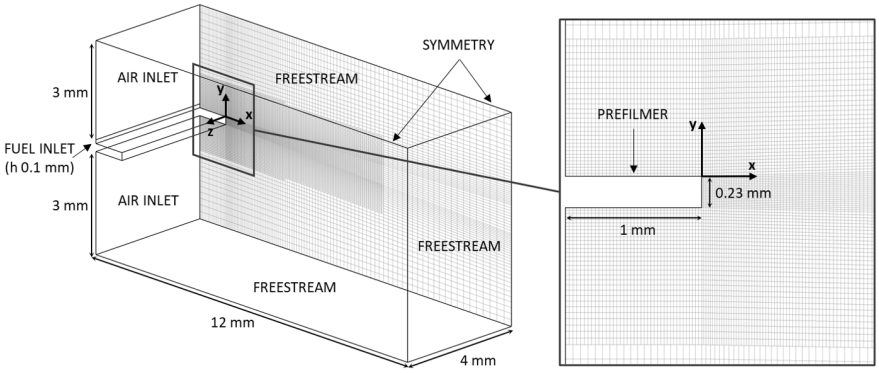

Figure 7: Numerical domain, reference frame, boundary conditions and employed mesh.

measured experimentally [5]. Lateral boundaries are modeled as symmetrical, while the remaining ones (top, bottom, outlet) are considered as freestream BCs.

The primary breakup requires a very fine mesh on the prefilmer surface and in the region near the lip. If the mesh resolution is high enough, the atomization process is well described, but it is not convenient in terms of computational effort. Consequently, in this study our focus is limited to a small region close to the prefilmer lip, where a fine hexahedral mesh has been used. Outside this zone, the size of the elements is doubled and it only serves to avoid the influence of boundary conditions on the relevant test-section. The final sizing for the cells near the prefilmer surface is 10.0 μm and the total number of cells is about 5.5 M elements.

Second order backward time scheme has been used for all quantities except for $\overline{\alpha}_l$. A special procedure called MULES was selected to preserve boundedness of this quantity [1]. The time step has been set to $1.5 \cdot 10^{-07}$ s. The *Wall Adapting Local Eddy viscosity* (WALE) model [28] has been employed to account for the effects of subgrid turbulent viscosity.

In Figure 8 left, the planes used for SMD computation are represented: the first one is located at the end of the prefilmer lip, while the last one is placed

6.00 mm downstream. The distance between each of them is 0.50 mm and, as already mentioned, they only extend in the refined mesh region. In Figure

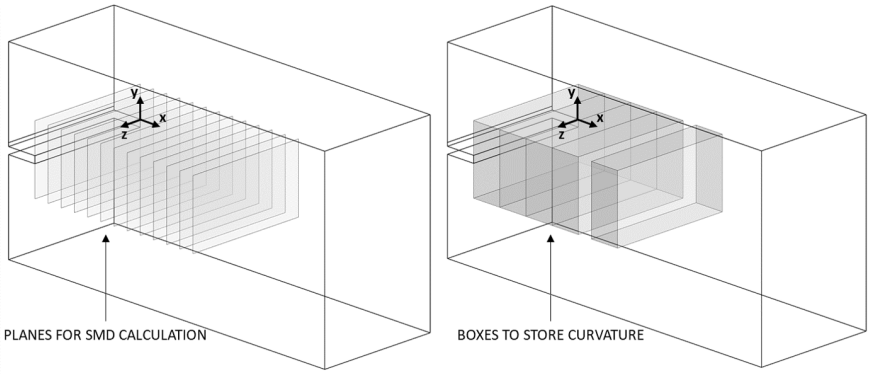

Figure 8: Post-processing locations: planes used to compute SMD (left) and boxes to store surface distribution in classes of curvature (right).

8 right, the boxes for curvature distribution storage are shown. In this work, boxes have been chosen to post process curvature distribution instead of plane used at run-time in order to limit the memory storage. In OpenFOAM ® the code has been adapted in order to store liquid/gas interface and curvature at each post processing time for any location.

4. Results on Sauter Mean Diameter and curvature distribution

4.1. Qualitative description

A qualitative outlook of the investigated phenomenon is provided in Figure 9, where two instantaneous isosurfaces at $\overline{\alpha}_l = 0.5$ are reported for the considered test case. It should be noticed that the chosen value of liquid volume fraction has the only purpose of visualize the main structures present at this point. Other iso-surface lower values would have shown much more liquid structures, since on this kind of representation of the interface that have a finite thickness all iso-surface does not collapse. Then the question that comes out is how to compile these information ? Any quantitative description reported

later considers all the iso-surfaces, each of those providing an element of surface that is finally integrated with the magnitude of the gradient of the liquid volume fraction as weighting factor.This standard approach has the advantage to be consistent when the interface thickness tends to zero. But of course when the interface is spread over to much numerical cells some characteristics of the interface can be lost.

In Figure 9, the main characteristics of this kind of atomization are represented by the simulation: the liquid flows from the inlet over the prefilmer surface, where some waves are generated due to the aerodynamic interaction with gaseous phase flowing above it. Later, the liquid is accumulated at the prefilmer lip (or trailing-edge) forming the so-called *reservoir*.

Here, the accumulated liquid is deformed and can eventually detach from the prefilmer. In Figure 9, two different events are shown in order to provide the reader a brief overview on the main structures that are generated during the primary breakup under the prescribed operating conditions. On the left side, the beginning of a *bag breakup* event can be identified: out of the reservoir a bag is formed which subsequently will burst, generating many small droplets [38]. On the right side, the formation of a ligament can be pointed out: ligaments will eventually detach from the reservoir, forming some spherical droplets under the effect of surface tension force.

It is out of the scope of this paper to describe in detail the atomization process and analyze how a simulation can reproduce the physical phenomena involved in primary breakup. This objective has already been very well accomplished in the previous works by Warncke et Al. [38], where `interFoam` is operated with a laminar approach (i.e., DNS), and by Braun et Al. [5], where SPH is used to reproduce in extreme details even the smallest liquid structures (in those two references air velocity was set to 50 m/s, while here the case at 40 m/s has been used).

From Figure 9, it is clear that the same spatial resolution of [38] and [5] is not achieved by the present calculation and only the largest liquid structures appear with the selected threshold of $\overline{\alpha}_l$. Indeed, Figure 9 also shows that the main

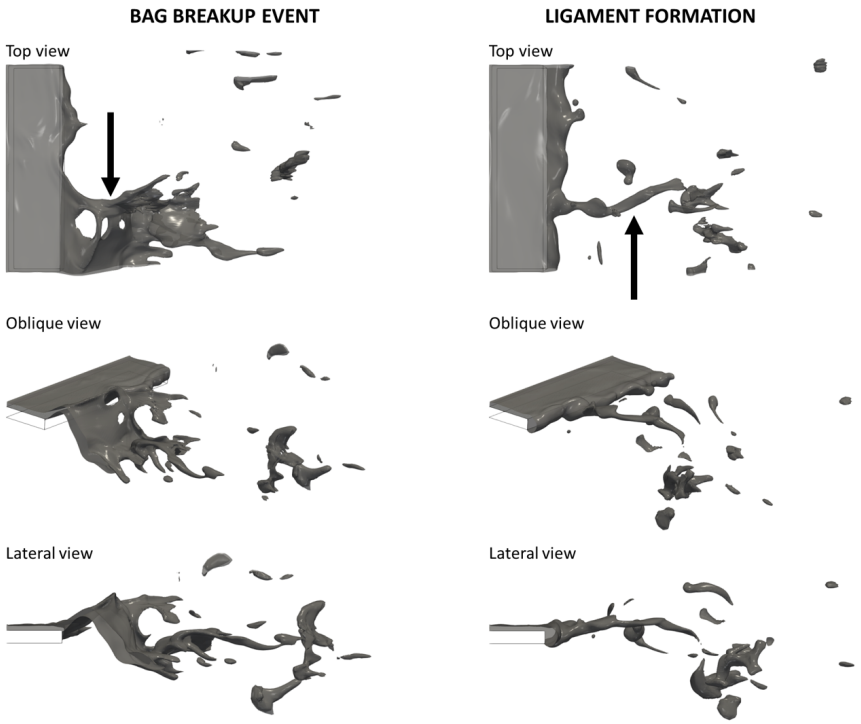

Figure 9: Qualitative representation of the investigated phenomenon, using an isosurface at $\overline{\alpha}_l = 0.5$: bag breakup event on the left, ligament formation on the right.

atomization features highlighted numerically [5, 9, 10, 38] and experimentally [16–18, 38] can still be identified with a relatively coarser mesh.

Indeed, the unique shortcoming that can be pointed out from the cited references is the very large amount of computational resources needed to carry out those simulations (approximately 540 kCPUhs in [38] and 3.6 MCPUhs in [5]). Therefore, their direct application to predict spray initial conditions for injection in an engineering context is not easy, although they surely represent a reference for scientific purposes.

Due to the engineering relevance of this work, a rather coarse mesh is here employed within the LES framework. In this way it is still possible to catch the most of liquid structures depicted so far by keeping the computational effort rel-

atively moderate. In fact, about 11 kCPUhs were necessary to run the present simulation for approximately the same physical time than [5, 38]. The original effort of the present work is to study which part of the physics has been kept with this less intensive simulation and to propose a methodology to determine spray characteristics.

4.2. SMD results

The results obtained using the post-processing methodology described in Section 2.2 are reported here. In Figure 10 the SMD has been computed for discrete planes at a given distance d_{lip} from the prefilmer injector lip using Equation 5 (planes are reported in Figure 8). It is worth recalling that only the region inside the refined mesh has been accounted for this computation (see Section 3.3).

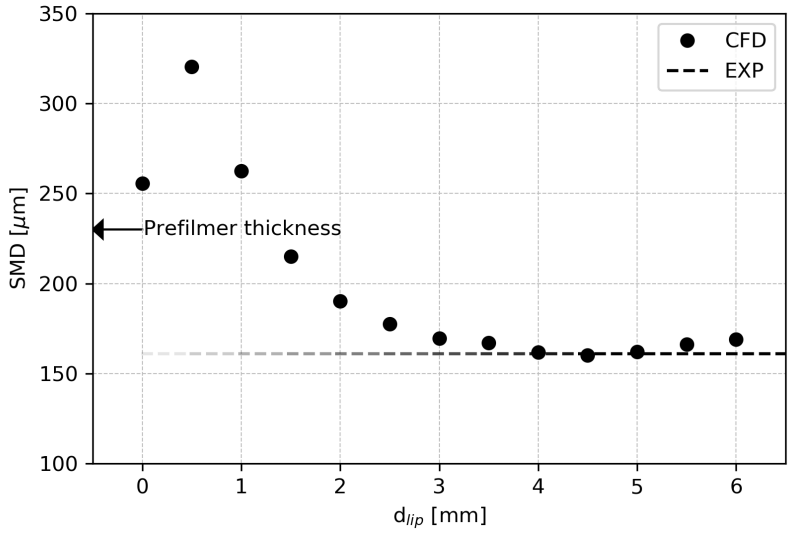

Figure 10: Axial variation of the SMD calculated over discrete planes at different distances from the injector (note that experimental datum is referred to the whole investigation window and cannot be attributed to a specific distance from the prefilmer lip, see Section 3.1).

The first point of the plot report the SMD in correspondence of the prefilmer trailing edge ($d_{lip} = 0.00$ mm): the predicted value (roughly 255 μm) is comparable with the prefilmer thickness (230 μm). Clearly, there is no point in defining a diameter of a mostly flat, coherent surface of liquid, whereas talking about a characteristic *length* would be more appropriate at this stage. But independently from the chosen nomenclature, such information could still be useful if the mass transfer in the dense region is of interest (see for instance [30]).

At $d_{lip} = 0.50$ mm the computed SMD is even higher than at $d_{lip} = 0.00$ mm and still larger than the prefilmer thickness. This may seems surprising since the SMD varies like the ratio of the liquid volume to the surface area. Thus, the fact that now the liquid have more interface (an upper and a lower one, as it is not in contact with the prefilmer anymore) is expected to reduce the SMD. But, a larger value is detected compared to the previous point at $d_{lip} = 0.00$ mm. In fact, there is an accumulation of the liquid behind the step of the prefilmer making the liquid sheet thickness greater than the film thickness causing an increase of the SMD that overtakes the effect of the doubling of surface. Of course, there is not yet any droplet at this stage and the SMD represents the characteristic size of the liquid sheet issued from the injector, not a diameter. Already at $d_{lip} = 1.00$ mm, the deformations of the liquid accumulation provide a lower SMD, which indicates the formation of smaller liquid structures that are stretched by the surrounding air flows, although they could still be attached to the reservoir (ligaments for instance).

At a higher axial distance from the prefilmer, the beginning of the primary breakup can be pointed out. From $d_{lip} = 1.50$ mm up to $d_{lip} = 3.00$ mm the predicted SMD strongly decreases: here, most of the primary breakup is taking place and smaller and smaller liquid structures are generated.

Moreover, it is important to note that even at these stages, non-spherical entities can be observed. However, the employed post-processing technique does not yet allow to distinguish between almost spherical droplets and non-spherical structures. This would be possible by exploiting the concept of Mean and Gauss curvatures already discussed in [7]. Anyway, it is important to notice that a

reduction in SMD is well recovered as expected.

Finally, from d_{lip} = 3.00 mm to d_{lip} = 6.00 mm, no major variations can be noticed. It indicates that most of the primary breakup takes place before, while in this zone the SMD stabilizes between 160.0 - 170.0 μm. Considering that the variation is limited, any of these planes could be used to predict the SMD of the spray that could be injected in a further combustion simulation.

The lower value of SMD is reached at a distance of d_{lip} = 4.50 mm (160.13 μm) while later a slight increase in SMD is observed. This could be due to the following phenomena:

- coalescence;
- stabilization of deformed liquid structures to become quiescent spherical droplets (lower amount of interface for the same amount of liquid volume);
- smallest structures flowing out of the considered refined zone;
- diffusion of the interface and transfer of smallest liquid entities to subgrid resolution.

All the cited phenomena could play a role, anyway it is important to highlight again how their effect is limited and would not strongly affect a separate simulation run with such SMD for spray injection. In the next sections, the SMD value (162.03 μm) computed at a distance of 5.00 mm from the lip will be used for further considerations, as done in [38].

Finally, in order to further validate the approach, the experimental datum is reported in Figure 10. Although the agreement could be considered extremely satisfying, it is worth pointing out how this value is computed from experiments as described in [16]. Instantaneous images are taken and spherical entities in the whole sampling window are identified using a dedicated algorithm, storing the detected diameter. Non-spherical liquid structures are instead discarded and not considered in for the calculation of the SMD. Finally, several independent images are analyzed and the SMD is computed based on the diameter assigned to the selected droplets. It is not possible to define a single axial distance where

the SMD is calculated for this experimental analysis that cover rather a zone where it is possible to detect droplets. A fading line is here plotted, meaning that the indicated value makes more sense moving farther from the trailing edge, where the primary breakup can be assumed to be established.

For the sake of clarity, the differences with the proposed numerical approach are pointed out:

- In experiments the full domain in considered while here probe planes at specified distances are used.
- It is still impossible to distinguish between almost-spherical and non-spherical entities, meaning that all the liquid structures are accounted for in the numerical calculation of the SMD.

Regarding the first point, we believe that the plateau shown in Figure 10 indicates that if additional breakup takes place downstream it leads to no major evolution of the SMD, thus making the two dataset comparable. On the second point, the work of Canu et al. [7] could help to address this issue. While small entities are more likely to have a spherical shape, the larger ones could still present relevant distortion. Identifying and not accounting for the largest non-spherical structures could produce a reduction in the calculated SMD, which would align the result of this work with the slight underprediction already noticed in [5] and [38].

To conclude, we believe that the comparison with experimental SMD is satisfactory even if not completely consistent. We believe that the present approach could be already employed to obtain a usefull and affordable prediction of the global SMD, to be used as a starting point for a subsequent simulation of the dilute spray in combustion simulation for instance.

If the spatial distribution of the SMD is of interest, then any other surface can be used in Equation 5 for recovering the spatial distribution (Figure 11). This information could be useful if a more refined injection is planned (using a non uniform value of SMD) or for validation purposes. In Figure 11, y denotes the component normal to the prefilming surface and y = 0.00 mm cor-

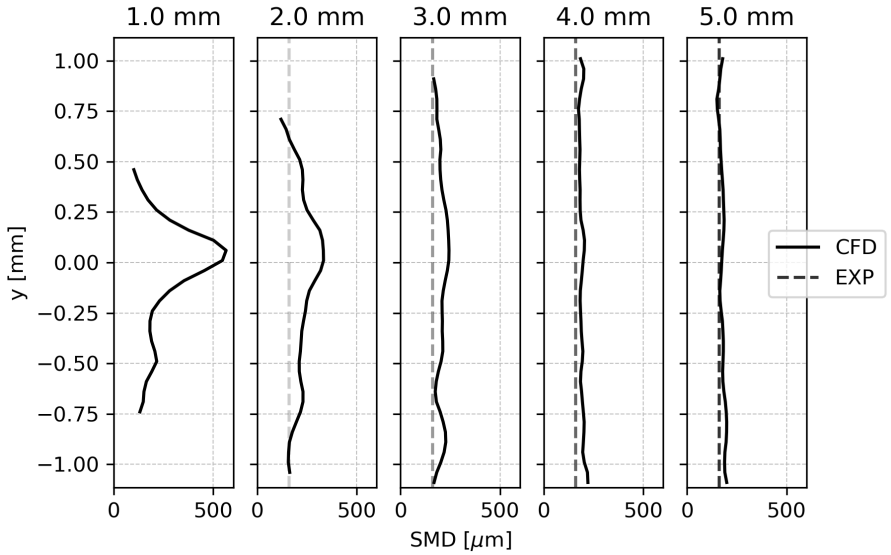

Figure 11: SMD distribution along vertical axis at specified distances from prefilmer lip d_{lip}, plotted only where time averaged liquid volume fraction is larger than 0.001 (note that no profile is available from experiments and the experimental line is plotted just for immediate reference.)

responds to the centre of the prefilmer trailing edge. Each plot is obtained at a given axial distance d_{lip} from the prefilmer trailing edge (similarly to Figure 10). The z direction in Equation 6, where the integration is performed, corresponds to the z coordinate in Figure 7. In order to discard the points where not enough liquid has been sampled, the lines are plotted only where time averaged $< \overline{\alpha}_l >_t \geq 0.001$.

At $d_{lip} = 1.00$ mm a large variation of the SMD can be observed along y, revealing that the largest liquid structures are still concentrated close to the prefilmer lip. Later ($d_{lip} = 2.00$ and $d_{lip} = 3.00$ mm) this peak starts to disappear. Finally, by analysing the same output at $d_{lip} = 4.00$ and $d_{lip} = 5.00$ mm, the SMD is almost uniformly distributed along the considered height.

Again, it is worth recalling that only a single value of SMD was available from the experiments referred to the whole investigation window. Therefore the ex-

perimental line shown in Figure 11 is not meant to directly compare with the numerical profiles, but only serves as reference to indicate that a reasonable prediction has been obtained.

To conclude, the presented analysis can be employed as a way to investigate the spatial progress of the atomization, by analysing the variation of the density of interface due to liquid structure arrangement. From the surface density it is possible to reconstruct a length scale that tends to a Sauter mean diameter that is compatible with the available experimental observation, despite a mesh resolution that is not has high as previous studies. This result may be surprising, since clearly the smallest length scale of the interface wrinkling are not as resolved than in the more refined studies. However, in the previous analysis both experimental and numeric have relied on the detection of complete droplet for which a diameter can be defined. Here, all parts of the surface is considering to contribute to the SMD estimation, thus a possibility exists that before a droplet is completely detached, it carries already the foot print of its feature diameter related to its volume to surface ratio. It is right also to insist on the definition of the SMD that is based on global integration that may hide the contribution of smallest droplet. Based on this consideration, it should be possible to provide a SMD map in space and time for spray injection in further simulation covering a larger domain but relying on dilute spray formulation, like in the present state of the art engine reactive simulations. By coupling the surface density and the curvature, it is also possible to access to the curvature distribution to enrich the description of the atomization process. This new postprocessing technique is the topic of the next section.

4.3. Curvature evolution

Once that SMD has been computed, a step forward would be to extract the spray size distribution: to this aim the curvature of the liquid/gas interface is firstly analyzed as described in Section 2.3. In Figure 12, the curvature distribution is plotted over the two instantaneous iso-surfaces already presented in Figure 9. The grey colour identifies the flat sections of the interface, that are

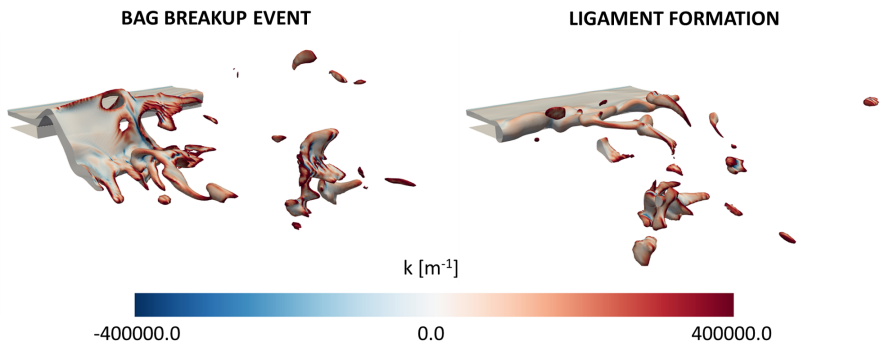

Figure 12: Curvature contour on iso-surfaces of $\overline{\alpha}_l = 0.5$. Bag breakup event on the left, ligamfigent formation on the right.

mainly located over the prefilmer and in some points over the bag (on the left). As expected, red (positive curvature, convex) zones are present where droplets or ligaments are formed, with a darker colour for smaller entities characterized by a larger curvature. It is important to note that also some blue points are visible, where concave surfaces are formed: even small entities, already detached from the prefilmer, can present some concave parts due to surface oscillation. Compared to the classical *diameter-based* description of the spray, a characterization based on curvature allows to continuously analyze the evolution of the liquid, from the initial dense region down to the final formation of dispersed droplets.

In Figure 13, the probability density function of the amount of interface for a given curvature is plotted for the different zones shown in Figure 8. As already stated, from now on this kind of plot will be referred as Surface Curvature Distribution or SCD. Again, it is worth recalling that only the flow inside the region with the fine mesh is considered (see again Figure 7 and 8). This is characterized by the two vertical dashed lines on both sides of the figure. They show the ultimate curvature that can be captured with the present mesh resolution. In order to better understand the ratio of the surface characterized by negative and positive curvature, the cumulative function of the SCD is also reported in

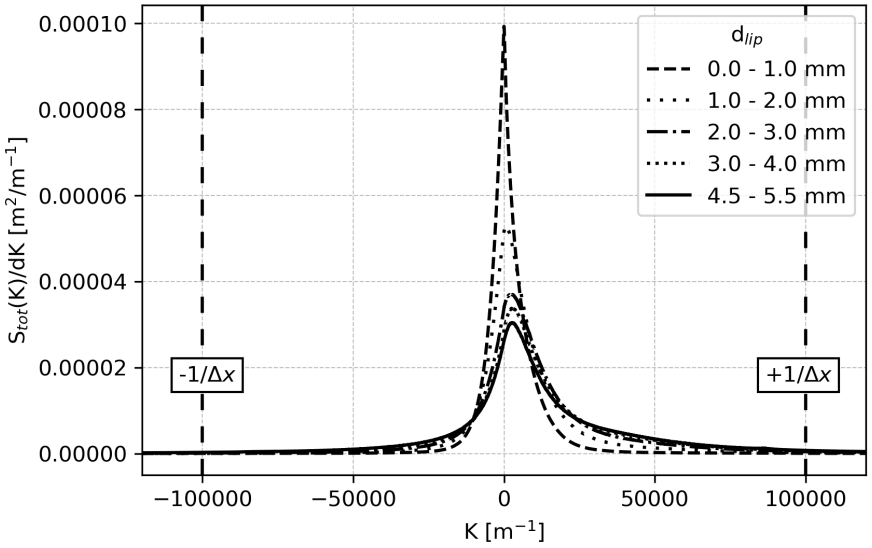

Figure 13: Probability density function of the amount of interface per classes of curvature (SCD) for four different boxes at a different distance from the prefilmer edge.

Figure 14 for the considered post-processing locations. In the first box, which extends from 0.00 up to 1.00 mm from the prefilmer edge, the peak of surface distribution is located close to K = 0 m^{-1}, meaning that most of the surface is actually *flat*. Also, both negative and positive values can be observed, which implies that both concave and convex structures can be identified in this area like waves traveling at the surface. From Figure 14, it can be observed that they carry almost the same amount of interface, since its cumulative function reports that about the 50% of the total surface can be found for $K \leq 0\ m^{-1}$.

In Figure 13 at d_{lip}: 1.00 - 2.00 mm it can be observed that the peak of the distribution is found for slightly positive K. At the same time, the convex (positive) side carries a larger amount of surface (Figure 14). This is consistent with the advance of the atomization process that produces droplets carrying mostly positive curvature. Some structures detach from the prefilmer trailing edge and due to the surface tension they tend to reshape for having convex surface like droplets or ligaments.

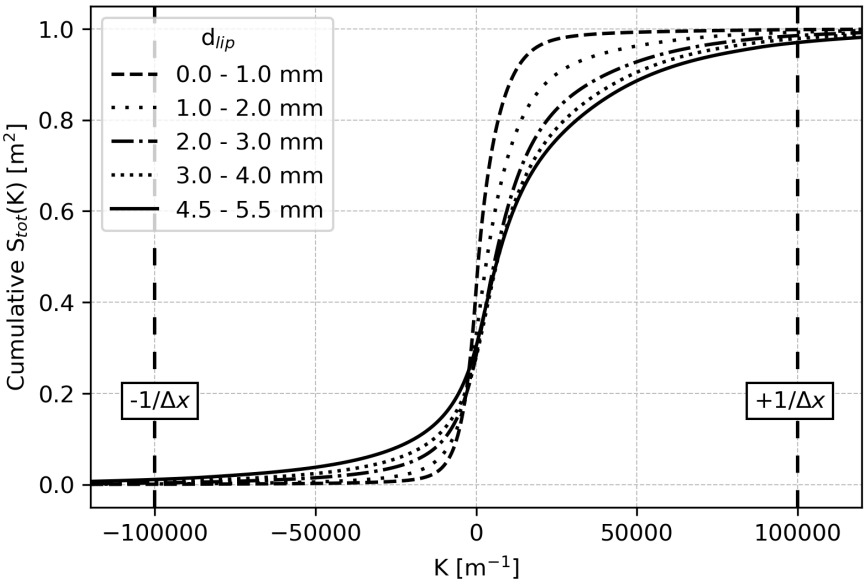

Figure 14: Cumulative function of the amount of interface per classes of curvature (SCD) for four different boxes at a different distance from the prefilmer edge.

This trend is confirmed also at the two successive locations (d_{lip}: 2.00 - 3.00 mm and d_{lip}: 3.00 - 4.00 mm), where the peak further moves towards positive values and there is a slight increase in the amount of surface associated to positive values. Moreover, the distribution gets wider and wider, meaning that more and more surface is *transported* by liquid structures with a larger curvature (both negative and positive). This implies that atomization is occurring and smaller entities are generated, which is also consistent with the observations made in the previous section regarding the SMD.

At the end of the refined zone, thus from 4.50 to 5.50 mm of distance from the injector d_{lip}, the farthest SCD is plotted on Figure 13 and 14 by a solid line. While the position of the peak is almost the same of the previous stage, a small tendency can still be seen in the widening of the distribution which has already been associated to the production of smaller structures. Anyway, the similarities with the two previous sampling locations imply that the atomization

process is not strongly progressing after d_{lip} = 3.00 mm.

It is not yet possible to perfectly define when primary breakup ends, but now it is possible to determine where it is the most efficient. We decided to use the last box (d_{lip}: 4.50 - 5.50 mm) to further continue our analysis on curvature distribution. At this stage, we associated the SMD value computed at the plane at d_{lip} = 5.00 mm (as in [38]), which lies in the middle of the considered box. A different distance can be considered but, given the small variations after 3.00 mm in both the SMD (Section 4.2) and in the SCD, the effect should be negligible. In the next section a new approach towards the prediction of the spray size distribution is explored based on the SCD.

5. Towards the prediction of the Drop Size Distribution

In the last section, it has been possible to measure the SCD and to show that it carries many information on the atomization and break-up processes. The SMD profiles have shown a stabilisation within the computational domain after d_{lip} = 3mm, in addition, the SCD starts to stabilize at the end of the computational domain as seen on Figure 13. So, the farthest position from the injector, where the SCD and the SMD are available will be used to the first attempt to determine the DSD. The main idea behind this attempt is to assume that the spray at this early stage is already carrying the main features of the DSD. Of course not many droplets are stabilised, but we want to test if we can extract from the surface the elements that are already compatible with the final DSD. It means that the surface carries already elements where the curvature is representative of the final curvature and thus of the final DSD. At this final stage, it will be possible to relate the SCD to the DSD by remarking that different classes of diameter can be defined corresponding to the curvature classes. Assuming that each parcel of surface is part of a sphere of the final spray, the relation between the diameter and the curvature will be $d_K = 4/K$. In addition, the SCD carry a certain amount of surface for each curvature and thus for each diameter. Traditionally, the DSD is mostly expressed in term of

number density. Thus, we have to provide the relation between each element of surface of the SCD and the corresponding number of droplets that can be used for the DSD. Still assuming that this surface element, characterized by an area A_K and a curvature K, is a part of a spherical droplet, then the corresponding number of droplet is simply given by:

$$n(d_K) = A_K/\pi d_K^2 \tag{8}$$

This approach is clearly a first approximation and other approaches using for instance Gauss-Bonet formula to distinguish liquid element that are homeomorphic to a sphere [26] or using both principal curvatures [7] are under development. For the present time, our purpose is just to build and test an approach based on numerical method already available on most of CFD code for liquid-gas flows that have an internal way to estimate the total curvature K. It is also clear that this relation (Equation 8) holds only for spherical droplets. This will be the case for the whole final spray, but at the axial stage where we have constructed the SCD, only a part of the surface is assumed to carry curvature relevant for the future spherical droplets. The last step of the method is thus to discard a part of the SCD to conserve only the element of surface for which the curvature distribution is already representative of the further spray. Clearly, many methods can be imagined to achieve this selection, again following the line developed in this work we begin with the simplest one.

The first consideration is to cancel the negative curvature, that for spherical object would have referred to a bubble. At this stage of the atomization process, there is clearly no or very few complete bubbles, but part of the surface carries negative curvature that can be associated to a piece of the bubble shell but that are more likely surface oscillations. Indeed, any wave will produce symmetrical amount of negative and positive curvature. We have though to introduce this symmetry to cancel the negative curvature part and the related positive one, but the symmetry is not really sure, thus we choose to simply discard the negative part. Then applying the Equation 8, we have recovered a DSD from which it has been possible to compute the SMD. As a result, we find a SMD more

than one order of magnitude bigger than the experimental reference value and the numerical SMD computed as the ratio of the liquid volume fraction to the surface density obtained in the previous section. By looking at the estimated DSD, we have observed that this over prediction of the SMD is due to the queue of the distribution for large diameters that contribute to increase drastically the mean diameter. The probability to find large diameters, coming back to the SCD, is related to the probability to encounter very small and positive curvature. Drawing the curvature on the surface like in Figure 12, the surface corresponding to this event has been found to be a nearly flat surface that belong to piece of liquid that are clearly not yet fully atomized. Thus the corresponding amount of surface does not carry yet the characteristics of the final spray and has not to be considered to predict the final DSD. Again several methods can be proposed, but we have simply decided to discard all the surface with a curvature less than a minimum value K_{min}. This value is an additional parameter than can be set to match the previously determined numerical SMD based on the liquid volume to surface ratio ($\frac{\Sigma}{\overline{\alpha_l}}$ obtained in the last section). Thus, the proposed method is still consistent and does not required any experimental information to predict the DSD.

In Figure 15 the DSD of the spray obtained with the proposed method is finally shown. As described in Section 2.3, DSD is obtained by transforming the classes of K into classes of diameter and by computing the number of droplets using the amount of surface area A_K. Then, in terms of diameter, negative and very high values are discarded using computed SMD as threshold as illustrated in Section 2.3.

Clearly the small diameter part of the DSD is truncated for two reasons: firstly, the mesh resolution is not high enough to capture the smallest diameters associated to high curvature; secondly the atomization process is not yet finalized. To illustrate the effect of the mesh resolution, the mesh resolution length scale (Δ_x) is reported on the figure by the dotted vertical line. However, the global shape of the distribution is representative of the distributions that are usually measured for this kind of spray. But a more quantitative analysis

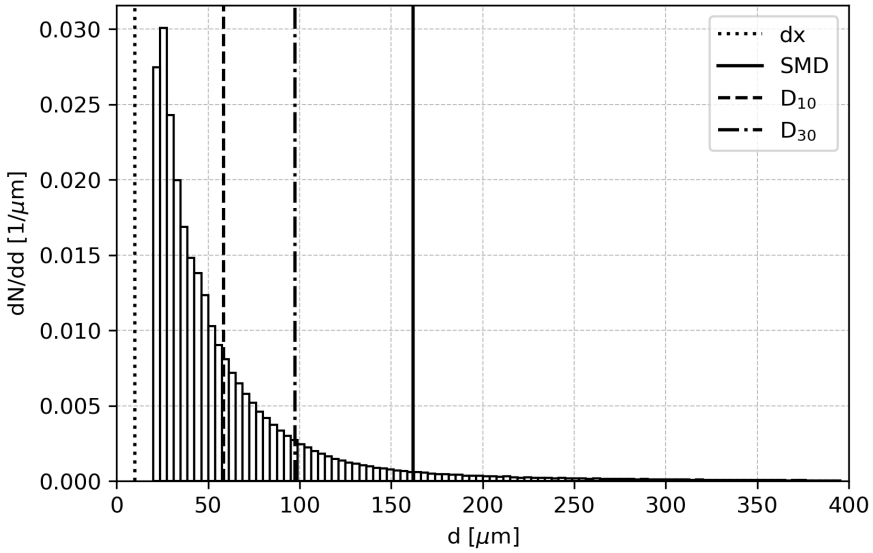

Figure 15: Final DSD applying the described post-processing procedure together with the different mean diameters illustrated with vertical lines

is carrying out by computing from this distribution the mean number diameter D_{10} and the mean volume diameter D_{30}, both together with the SMD are drawn as vertical lines. The corresponding values are reporter in the table below.

Table 2: Main diameters.

	Experimental	Σ	K clipped
$SMD\,[\mu m]$	161.00	162.03	161.94
$D_{10}\,[\mu m]$	56.80	-	58.35
$D_{30}\,[\mu m]$	97.55	-	97.49
Limits $[\mu m]$	-	-	0.0 - 396.83
Location	full window	plane at 5.00 mm	box from 4.5 to 5.5 mm

An remarkable agreement with the experimental data is found. It is interesting to notice that while the SMD is forced to be the same by cutting the tail

of the DSD using the SMD obtained from Σ (which already had a fair agreement with the experimental one), both D_{10} and D_{30} are comparable between experiments and numerical simulation. We are not claiming this is the method to be used to estimate spray distribution numerically. But we think that this approach has some potentials that can be interested to share with the scientific community.

6. Conclusions

In this work, the numerical investigation of a prefilming airblast atomizer has been carried out using the coupled ICM-ELSA approach and applying a novel technique to postprocess the results based on distributed variables such as the curvature of the liquid interface. The novelty of this approach relies on the post-processing and the related analysis. This test case have been already used for high fidelity simulations that aim to catch nearly all the feature of the atomization up to the final formation of the spray. Here, we use in purpose a less intensive computational strategy that is not able to follow the spray formation with all the its details but that is still able to catch the mains mechanisms of breakup. Also, the computational effort is reduced because the final stage of breakup that forms and stabilises the spherical droplet is not considered. However, it is possible to access to global characteristic of spray like the mean liquid volume fraction and the mean surface density from which it is possible to compute the SMD through several planes locates at different distance from the injector. This SMD is for a spray the ratio between the liquid volume to the liquid-gas surface. Thus this SMD can be estimated even for non spherical droplets and in fact for any interface morphology, leading to a characteristic length since no diameter can be defined. Thus, the evolution of this SMD, has been computed all along the atomization process and its evolution has been discussed with respect to the liquid structure we can observe in the simulation. Due to the break up, this quantity mainly decreases and then it reaches a plateau. This plateau is reached before the finalisation of the atomization, meaning that

the main production of the liquid-gas interface is achieved suddenly and then the SMD is less sensitive to the final formation of droplet. The value reached in such plateau is also in good agreement with the experimental data, showing that the small scale events that are necessarily missed with our reduced approach are not affecting too much this quantity.

Then we analysed the atomization process through the interface curvature distribution. Both negative and positive values are found, indicating the presence of both convex and concave element of surface. Closer to the atomizer, the reported distribution is almost symmetrical and very narrow. Here the peak is located close to $K = 0$, which means that most of the surface is flat. Downstream, the peak of the PDF moves towards positive values, because of the liquid detachment from the prefilmer trailing edge and progressive reshaping into convex entities that will becomes droplets. At the same time, the distribution becomes wider and wider, signing the creation of droplets with a smaller diameter. This is consistent with the progress of the atomization process and with the conclusions drawn thanks to the SMD.

Finally, a first attempt to recover the spray DSD from the curvature distribution has been tested. Starting from the interface distribution per classes of curvature, negative curvature values have been discarded. At this stage, the conversion from SCD to DSD is carried out. The resulting DSD results in a very high SMD, because there are surface elements with very small curvature occurring where the interface is nearly flat. Thus, they lead to equivalent very large diameter of droplet that affect the SMD estimation. In this work, we addressed this issue by clipping the tail of the DSD in order to recover the global SMD value obtained as the ratio of the liquid volume fraction to the surface density. We arrive to a shape of the DSD that seems reasonable with respect those propose in the literature, even if the small scale diameter are missing due to the reduced mesh resolution. We can imagine to complete the tail of the DSD for small diameter with ad-hoc model, but here we simply neglect them. Finally, we test the DSD obtained from this analysis by computing the D_{10} and D_{30} that have been measured experimentally and we have found a remarkable agreement,

which validates the computed DSD. We are conscious that the analysis of the SCD to predict the DSD is a first attempt that requires further confirmation. Hence, future works will be devoted to further validate this approach, for instance by investigating different geometrical configurations or studying different operating conditions.

Overall, the proposition is that the interface carries surface elements already representative of the final spray even at early stage of atomization. To determine which element is representative of the final spray, we have propose a simple approach that could be improved in many way. One important part of the reasoning is to filter the measured curvature distribution to make it consistent with more global quantity such as the liquid volume fraction and the surface density here by using the SMD. This approach clearly cannot be considered yet a general-purpose methodology for determining the spray characteristics. Nevertheless, even if it is at preliminary stage, we find on the test case under investigation a very encouraging agreement with respect to available experimental data. This push us to share this idea with the scientific community, for those that would be interested to test it. It would be interested also to test it from an experimental point of view so to see if indeed the surface contains element of the final spray at early stage. It is hard at this level to determine what means exactly early stage. From our simulation, we think this relates to the axial distance where the SMD is stabilized: where we find a plateau or at least a minimum value.

To conclude, we have studied the atomization process from a well known configuration that has been investigated previously with high fidelity simulations. We have studied if it is possible through new analysis to get information on the spray with less intensive numerical simulation. The analysis of liquid volume fraction and surface density leads to a correct prediction of the SMD that can be complete by the analysis of the SCD to predict the diameter spray distribution.

Acknowledgements

The authors gratefully acknowledge Dr. Ing. Rainer Koch and Dr. Geoffrey Chaussonnet for sharing the results of their experimental campaign.

Appendix 1

The requirement of a preliminary single-phase simulations has already been highlighted in Section 3.2 and demonstrated by [38, 39].

Compared to [38, 39], in this work a different strategy has been adopted: starting from the single-phase LES simulation of the whole prefilmer apparatus, the velocity data history has been sampled on a proper plane and subsequently applied to a channel with a finer zonal grid close to the walls to enhance the resolution of the velocity profiles in the boundary layer. Finally, the velocity field has been sampled again at the channel outlet and imposed as time-varying inlet condition of the embedded multiphase simulation.

Conversely, in [38, 39] the single-phase LES simulation has been directly performed on the so-called *turbulent channel*. However, the direct use of this data leads to the lack of the temporal history of the flow field related to the prefilmer itself. In fact, the resulting profiles would be more affected by the modelling assumption at the inlet of the turbulent channel (i.e. the turbulence intensity at the inlet and the chosen sub-grid model) than the effective geometry of the test case.

Instead, the strategy adopted here does not apply directly a turbulence generator to the channel inlet, but a flow-field obtained from a simulation representative of the whole domain.

As in [38, 39], the obtained velocity profiles have been employed in the multiphase simulation.

Step 1: Single-phase simulation of the whole domain

The first step involves a single-phase simulation of the whole prefilmer in order to recover a more realistic flow-field for the carrier phase. The elements

are hexaedral with a base sizing equal to 0.5 mm, while a mesh grading has been applied on the prefilmer lip to further refine the mesh in this area. The total number of elements amounts to 4.7 M.

The simulation employs second order schemes for the momentum and a Smagorinsky model to account for the sub-grid scales of turbulence. A mean velocity of 40.0 m/s has been applied to the inlet boundary and a turbulence intensity of approximately 10 % has been superimposed to generate velocity fluctuations. However, due to the very small size of the eddies close to the wall and involved in the atomization process, such step was not sufficient for a proper prediction of the velocity profiles to be used in the multiphase simulation. In order to contain the computational cost of the single-phase simulation, this mesh has not been further refined and the improvement of such profiles has been obtained with the following step.

Step 2: channel flow

With the aim of enhancing the resolution of velocity profiles, the stored velocity history of Step 1 has been applied to channel. This domain is characterized by a progressive mesh refinement moving from the central freestream region towards the walls. Hence, the velocity profiles have been collected again on the outlet plane in time.

The channel presents a rectangular section where the cell sizing ranges from 200 μm in the freestream up to 50 μm near the wall. To this aim, two refinement steps have been performed, each of which halves the previous sizing, leading to a final amount of 5.35 M elements. The simulation employs the same modelling choices of Step 1.

Moving from the inlet to the outlet, the flow-field becomes more *turbulent* close to the wall and the overall defintion of local eddies is increased. This clearly leads to a more realistic prediction of the atomization process due to the absence of strong assumption on the boundary layer.

The achieved velocity profiles are finally sampled at the outlet, providing a suitable temporal window for the subsequent multiphase simulation.

References

[1] Anez, J., Ahmed, A., Hecht, N., Duret, B., Reveillon, J., Demoulin, F.X., 2018. Eulerian–Lagrangian spray atomization model coupled with interface capturing method for diesel injectors. International Journal of Multiphase Flow URL: https://doi.org/10.1016/j.ijmultiphaseflow.2018.10.009, doi:10.1016/j.ijmultiphaseflow.2018.10.009.

[2] Anez, J., Puggelli, S., Hecht, N., Andreini, A., Reveillon, J., Demoulin, F.X., 2019. Liquid Atomization Modeling in OpenFOAM, in: OpenFOAM®. Springer International Publishing, Cham, pp. 297–308. URL: http://link.springer.com/10.1007/978-3-319-60846-4{_}22, doi:10.1007/978-3-319-60846-4_22.

[3] Beheshti, N., Burluka, A.A., Fairweather, M., 2007. Assessment of Σ-Y_{liq} model predictions for air-assisted atomisation. Theoretical and Computational Fluid Dynamics 21, 381–397. URL: http://link.springer.com/10.1007/s00162-007-0052-3, doi:10.1007/s00162-007-0052-3.

[4] Brackbill, J., Kothe, D., Zemach, C., 1992. A continuum method for modeling surface tension. Journal of Computational Physics 100, 335–354. doi:https://doi.org/10.1016/0021-9991(92)90240-Y.

[5] Braun, S., Wieth, L., Holz, S., Dauch, T.F., Keller, M.C., Chaussonnet, G., Gepperth, S., Koch, R., Bauer, H.J., 2019. Numerical prediction of air-assisted primary atomization using Smoothed Particle Hydrodynamics. International Journal of Multiphase Flow 114, 303–315. URL: https://linkinghub.elsevier.com/retrieve/pii/S0301932218304087, doi:10.1016/j.ijmultiphaseflow.2019.03.008.

[6] Canu, R., Duret, B., Reveillon, J., Demoulin, F.X., 2020. Curvature-based interface resolution quality (irq) indicator to assess simulation accuracy. Atomization and Sprays 30, 31–53. doi:10.1615/AtomizSpr.2020033923.

[7] Canu, R., Puggelli, S., Essadki, M., Duret, B., Menard, T., Massot, M., Reveillon, J., Demoulin, F.X., 2018. Where does the droplet size distribution come from? International Journal of Multiphase Flow 107, 230–245. URL: http://www.sciencedirect.com/science/article/pii/S0301932218302854, doi:https://doi.org/10.1016/j.ijmultiphaseflow.2018.06.010.

[8] Chaussonnet, G., Gepperth, S., Holz, S., Koch, R., Bauer, H.J., 2020. Influence of the ambient pressure on the liquid accumulation and on the primary spray in prefilming airblast atomization. International Journal of Multiphase Flow 125, 103229. doi:10.1016/j.ijmultiphaseflow.2020.103229, arXiv:1906.04042.

[9] Chaussonnet, G., Riber, E., Vermorel, O., Cuenot, B., Gepperth, S., Koch, R., 2013. Large Eddy Simulation of a prefilming airblast atomizer, in: ILASS – Europe 2013, 25th European Conference on Liquid Atomization and Spray Systems, Chania, Greece, 1-4 September 2013, pp. 1–4.

[10] Chaussonnet, G., Vermorel, O., Riber, E., Cuenot, B., 2016. A new phenomenological model to predict drop size distribution in Large-Eddy Simulations of airblast atomizers. International Journal of Multiphase Flow 80, 29–42. URL: http://dx.doi.org/10.1016/j.ijmultiphaseflow.2015.10.014, doi:10.1016/j.ijmultiphaseflow.2015.10.014.

[11] Cuenot, B., 2016. Gas Turbines and Engine Simulations, in: Advances in Chemical Engineering, Volume 49. 1 ed.. Elsevier Inc.. volume 49, pp. 273–385. URL: http://dx.doi.org/10.1016/bs.ache.2016.09.004https://linkinghub.elsevier.com/retrieve/pii/S0065237716300175, doi:10.1016/bs.ache.2016.09.004.

[12] Desantes, J.M., García-Oliver, J.M., Pastor, J.M., Pandal, A., Baldwin, E., Schmidt, D.P., 2016. Coupled/decoupled spray simulation comparison of the ECN spray a condition with the σ-Y Eulerian atomization

model. International Journal of Multiphase Flow 80, 89–99. doi:10.1016/j.ijmultiphaseflow.2015.12.002.

[13] Deshpande, S.S., Anumolu, L., Trujillo, M.F., 2012. Evaluating the performance of the two-phase flow solver interFoam. Computational Science & Discovery 5, 014016. URL: http://stacks.iop.org/1749-4699/5/i=1/a=014016?key=crossref.48e889e2d1a207d9665630feb80f2a41https://iopscience.iop.org/article/10.1088/1749-4699/5/1/014016, doi:10.1088/1749-4699/5/1/014016.

[14] Ding, J.W., Li, G.X., Yu, Y.S., Li, H.M., 2016. Numerical Investigation on Primary Atomization Mechanism of Hollow Cone Swirling Sprays. International Journal of Rotating Machinery 2016. doi:10.1155/2016/1201497.

[15] ECN, 2019. Engine Combustion Network. URL: https://ecn.sandia.gov/.

[16] Gepperth, S., Guildenbecher, D.R., Koch, R., Bauer, H.J., 2010. Prefilming primary atomization: Experiments and modeling, in: ILASS – Europe 2010, 23rd Annual Conference on Liquid Atomization and Spray Systems, Brno, Czech Republic, September 2010, p. 0.

[17] Gepperth, S., Koch, R., Bauer, H.J., 2013. Analysis and Comparison of Primary Droplet Characteristics in the Near Field of a Prefilming Airblast Atomizer, in: Volume 1A: Combustion, Fuels and Emissions, American Society of Mechanical Engineers. p. 0. URL: https://asmedigitalcollection.asme.org/GT/proceedings/GT2013/55102/SanAntonio,Texas,USA/249787, doi:10.1115/GT2013-94033.

[18] Gepperth, S., Müller, A., Koch, R., Bauer, H., Strömungsmaschinen, T., Institut, K., 2012. Ligament and Droplet Characteristics in Prefilming Airblast Atomization, in: ICLASS 2012, 12th Triennial International Conference on Liquid Atomization and Spray Systems, Heidelberg, Germany, September 2-6, 2012, p. 0.

[19] Giusti, A., Mastorakos, E., 2019. Turbulent Combustion Modelling and Experiments: Recent Trends and Developments. Flow, Turbulence and Combustion 103, 847–869. doi:10.1007/s10494-019-00072-6.

[20] Herrmann, M., 2010. Detailed Numerical Simulations of the Primary Atomization of a Turbulent Liquid Jet in Crossflow. Journal of Engineering for Gas Turbines and Power 132, 1–10. doi:10.1115/1.4000148.

[21] Kindlmann, G., Whitaker, R., Tasdizen, T., Moller, T., 2003. Curvature-based transfer functions for direct volume rendering: methods and applications, in: IEEE Visualization, 2003. VIS 2003., pp. 513–520.

[22] Lefebvre, A., McDonell, V., 2017. Atomization and Sprays, Second Edition. URL: https://www.crcpress.com/Atomization-and-Sprays-Second-Edition/Lefebvre-McDonell/p/book/9781498736251, doi:10.1016/0009-2509(90)87140-N.

[23] Leung, T.F., Groth, C.P., Hu, J., 2017. Evaluation of an Eulerian-Lagrangian Spray Atomization (ELSA) Model for Nozzle Flow: Modeling of Coupling Between Dense and Disperse Regions. 47th AIAA Thermophysics Conference , 1–14doi:10.2514/6.2017-4352.

[24] Martí-Aldaraví, P., Pastor, J.M., 2019. Review of an Eulerian Σ-Y Spray Atomization Model for Nozzle Flow and Near-Field Diesel Spray Modeling, in: Two-Phase Flow for Automotive and Power Generation Sectors. Springer Singapore, pp. 9–42. URL: http://link.springer.com/10.1007/978-981-13-3256-2http://link.springer.com/10.1007/978-981-13-3256-2{_}2, doi:10.1007/978-981-13-3256-2_2.

[25] Ménard, T., Tanguy, S., Berlemont, A., 2007. Coupling level set/VOF/ghost fluid methods: Validation and application to 3D simulation of the primary break-up of a liquid jet. International Journal of Multiphase Flow 33, 510–524. URL: https://linkinghub.elsevier.com/

retrieve/pii/S0301932206001832, doi:10.1016/j.ijmultiphaseflow.2006.11.001.

[26] Mohamed, E., Florence, D., de Chaisemartin Stéphane, Adam, L., Thibault, M., Marc, M., 2019. Statistical modeling of the gas–liquid interface using geometrical variables: Toward a unified description of the disperse and separated phase flows. International Journal of Multiphase Flow 120, 103084. URL: http://www.sciencedirect.com/science/article/pii/S0301932217308583, doi:https://doi.org/10.1016/j.ijmultiphaseflow.2019.103084.

[27] Nambu, T., Mizobuchi, Y., 2020. Detailed numerical simulation of primary atomization by crossflow under gas turbine engine combustor conditions. Proceedings of the Combustion Institute 000, 1–9. doi:10.1016/j.proci.2020.06.067.

[28] Nicoud, F., Ducros, F., 1999. Subgrid-scale stress modelling based on the square of the velocity gradient tensor. Flow, Turbulence and Combustion 62, 183–200. URL: https://doi.org/10.1023/A:1009995426001, doi:10.1023/A:1009995426001.

[29] Ning, W., Reitz, R.D., Diwakar, R., Lippert, A.M., 2009. An eulerian-lagrangian spray and atomization model with improved turbulence modeling. Atomization and Sprays 19, 727–739. doi:10.1615/AtomizSpr.v19.i8.20.

[30] Palanti, L., Puggelli, S., Andreini, A., Reveillon, J., Duret, B., Demoulin, F.X., 2020. An implicit formulation to model the evaporation process in the ELSA framework. Atomization and Sprays 29, 1043–1069. URL: http://dl.begellhouse.com/journals/6a7c7e10642258cc,forthcoming,32627.html, doi:10.1615/AtomizSpr.2020032627.

[31] Rosenfeld, A., Pfaltz, J.L., 1966. Sequential Operations in Digital Picture Processing. Journal of the ACM (JACM) doi:10.1145/321356.321357.

[32] Sanjosé, M., Senoner, J.M., Jaegle, F., Cuenot, B., Moreau, S., Poinsot, T., 2011. Fuel injection model for Euler-Euler and Euler-Lagrange large-eddy simulations of an evaporating spray inside an aeronautical combustor. International Journal of Multiphase Flow 37, 514–529. doi:10.1016/j.ijmultiphaseflow.2011.01.008.

[33] Sauer, B., Sadiki, A., Janicka, J., 2014. Numerical Analysis of the Primary Breakup Applying the Embedded DNS Approach to a Generic Prefilming Airblast Atomizer. The Journal of Computational Multiphase Flows 6, 179–192. URL: http://journals.sagepub.com/doi/10.1260/1757-482X.6.3.179, doi:10.1260/1757-482X.6.3.179.

[34] Sauer, B., Sadiki, A., Janicka, J., 2016. EMBEDDED DNS CONCEPT FOR SIMULATING THE PRIMARY BREAKUP OF AN AIRBLAST ATOMIZER. Atomization and Sprays 26, 187–215. URL: http://www.dl.begellhouse.com/journals/6a7c7e10642258cc,54cdd3533559658c,352d2d9147d245bd.html, doi:10.1615/AtomizSpr.2014011019.

[35] Shao, C., Luo, K., Yang, Y., Fan, J., 2017. Detailed numerical simulation of swirling primary atomization using a mass conservative level set method. International Journal of Multiphase Flow 89, 57–68. doi:10.1016/j.ijmultiphaseflow.2016.10.010.

[36] Shinjo, J., 2018. Recent Advances in Computational Modeling of Primary Atomization of Liquid Fuel Sprays. Energies 11, 2971. doi:10.3390/en11112971.

[37] Trask, N., Schmidt, D.P., Lightfoot, M., Danczyk, S., 2012. Compressible Modeling of the Internal Two-Phase Flow in a Gas-Centered Swirl Coaxial Fuel Injector. Journal of Propulsion and Power 28, 685–693. URL: http://arc.aiaa.org/doi/abs/10.2514/1.B34102http://arc.aiaa.org/doi/10.2514/1.B34102, doi:10.2514/1.B34102.

[38] Warncke, K., Gepperth, S., Sauer, B., Sadiki, A., Janicka, J., Koch, R., Bauer, H.J., 2017. Experimental and numerical investigation of the primary breakup of an airblasted liquid sheet. International Journal of Multiphase Flow 91, 208–224. URL: http://dx.doi.org/10.1016/j.ijmultiphaseflow.2016.12.010https://linkinghub.elsevier.com/retrieve/pii/S0301932215302147, doi:10.1016/j.ijmultiphaseflow.2016.12.010.

[39] Warncke, K., Sadiki, A., Janicka, J., 2019. New insights in the role of turbulence for simulating primary breakup of prefilming airblast atomization, in: ILASS - Europe 2019, 29th European Conference on Liquid Atomization and Spray Systems, Paris. p. 0.

[40] Xue, Q., Battistoni, M., Powell, C.F., Longman, D.E., Quan, S.P., Pomraning, E., Senecal, P.K., Schmidt, D.P., Som, S., 2015. An Eulerian CFD model and X-ray radiography for coupled nozzle flow and spray in internal combustion engines. International Journal of Multiphase Flow 70, 77–88. URL: http://dx.doi.org/10.1016/j.ijmultiphaseflow.2014.11.012, doi:10.1016/j.ijmultiphaseflow.2014.11.012.

Highlights:

- Numerical simulation of the atomization occurring in an air blast atomizer
- Numerical determination of the amount of liquid-gas surface along that atomization process.
- Numerical determination of the surface curvature distribution along the atomization process.
- A new approach is proposed to obtain the drop size distribution from curvature distribution and liquid volume fraction
- This approach allows the determination of the spray size distribution at an early stage of the atomization process.

Reviewing and Editing.
Stefano Puggelli: Conceptualization, Investigation, Methodology, Software, Validation, Writing- Reviewing and Editing.
Leonardo Langone: Conceptualization, Investigation, Methodology, Software, Validation, Writing- Reviewing and Editing.
Antonio Andreini: Supervision, Conceptualization, Investigation, Methodology, Software, Validation, Funding acquisition, Writing- Reviewing and Editing, Resources.
Julien Reveillon: Supervision, Conceptualization, Investigation, Methodology, Software, Validation, Funding acquisition, Writing- Reviewing and Editing, Resources.
Benjamin Duret: Supervision, Conceptualization, Investigation, Methodology, Software, Validation, Funding acquisition, Writing- Reviewing and Editing, Resources.
François-Xavier Demoulin: Supervision, Conceptualization, Investigation, Methodology, Software, Validation, Funding acquisition, Writing- Reviewing and Editing, Resources.

Declaration of interests

☒ The authors declare that they have no known competing financial interests or personal relationships that could have appeared to influence the work reported in this paper.

☐The authors declare the following financial interests/personal relationships which may be considered as potential competing interests: